Measurements of UWB Propagation and Transmission for Wireless Links in Spacecrafts

Miyuki Hirose and Takehiko Kobayashi
Wireless Systems Laboratory
Tokyo Denki University
Tokyo, Japan
miyuki@wsl.c.dendai.ac.jp

***Abstract*—This paper presents measurement and characterization of ultra wideband propagation with a view to (at least partly) replacing wired interface buses in spacecrafts with wireless links. Channel responses in the frequency- and time-domain, spatial distributions of UWB and narrowband propagation gains, delay spreads, and throughputs were measured with use of four different-sized shield boxes (simulating miniature satellites). In terms of Frequency domain, narrowband resulted in nearly 35-dB fading at several "dead spots" caused by multipath environment, UWB yielded none. However, significantly long delay spreads and thus limited link performance are caused by multipaths within a conductive enclosure. Even in such an environment, it was found that delay spreads can be suppressed by partially paneling a radio absorber and apertures (perforated on the outer surface of satellites). The results revealed that commercially-available UWB devices were capable of accommodate up to 480-Mb/s data buses within spacecrafts.**

Keywords- intra-spacecraft wireless communication; urtra-wideband; radio propagation; delay spreads.

I. INTRODUCTION

Recently, a number of studies have been reported about wireless communications in closed and semi-closed environments [1]-[4]. We proposed wireless communication within a spacecraft for replacing wired interface buses with wireless links and experimentally studied ultra wideband (UWB) radio propagation in a small scientific spacecraft [5]. Narrowband wireless links within a spacecraft were numerically calculated and evaluated in [6]. However, narrowband wireless communication systems cause spatial fading in multipath environments and therefore need a substantial amount of fading margin. On the other hand, UWB signals suffer less from multipath fading, and thus provide more dependable, higher-speed links (e.g., maximum of 400 Mb/s per node attained with SpaceWire [7], equaling the standards of a wired onboard data bus).

As on-board mission equipment diversifies, the volume and weight of cable used to interconnect subsystems increase. Since data buses used in manned spacecrafts are required to be tripled, the weight becomes further significantly heavy. Moreover, spacecrafts have been assembled manually for the most part, resulting in high costs and long lead times. Particularly, harnessing, interconnecting, and testing interface buses have been becoming much more time-consuming, as spacecraft complexity increases [8]. Although wireless technologies have not been utilized within spacecrafts as a physical layer of data buses, applying wireless technologies to a portion of signal wires could be extremely useful. A use of wireless connections within the spacecrafts could contribute to: (i) reduction of cable weight and launching cost as a result, (ii) reduction in the cost of manufacture, and (iii) more flexibility in layout of spacecraft subsystems, and (iv) more reliable connections at rotary, moving, and sliding joints. In this study, UWB signal propagation was measured (3.1 — 10.6 GHz, the full-band UWB, 4.2 — 4.8 GHz, a part of the low-band UWB proved in Japan, and 7.4 — 7.9 GHz, a part of the high-band UWB approved in Japan) in a shield box. In Section II, our experiment setup was presented. Measurement results of propagation and transmission are described in Section III and IV respectively. Section V concludes the paper.

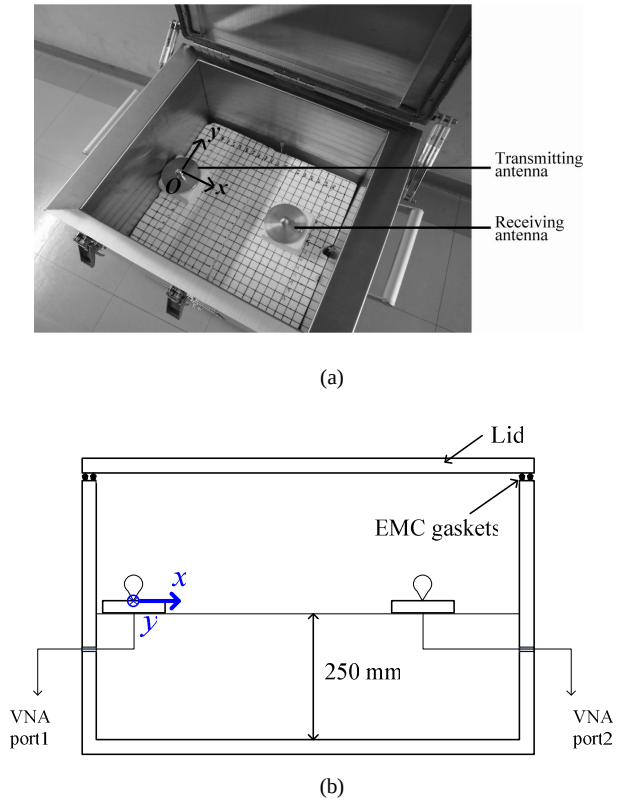

Figure 1. Measurement setup in a shield box: (a) top and (b) side views.

 ISBN: 978-1-61208-453-4

II. EXPERIMENT SETUP

A shield box, 430 mm long × 470 mm wide × 435 mm high, simulating a small scientific spacecraft "INDEX/REIMEI" (launched in 2005) was used for the measurements. Within the shield box, the transmitting antenna was fixed at 250 mm above the bottom and adjacent to the center of a 430-mm side, as shown in Fig. 1. This position was defined as the origin of the Cartesian coordinate, whose x and y axes were parallel to the sides. The receiving antenna was scanned within a region $0 \le x$ [mm] ≤ 340 and $-140 \le y$ [mm] ≤ 140 in 20-mm intervals on a polystyrene foam stage (virtually transparent to microwave). Since the minimum distance between the antenna electric centers was 120 mm < $\lambda_L / 2\pi$ (λ_L is the wavelength at the lowest frequency), all the measurements were carried out in a far-field region. The transmitting and receiving antennas were omnidirectional, vertically polarized, low voltage-standing-wave-ratio UWB monopole antennas [5]. Their circular ground planes were 100 mm in diameter. During the measurements, the conductive top lid was closed.

Frequency- and time-domain propagation gains were measured with a microwave vector network analyzer (VNA). Major specifications of the measurements are listed in Table I. From the frequency-domain power gain data, the UWB propagation gains were calculated by summing the power of the gains between the feeding points of the antennas over the occupied bandwidth:

$$PG_{UWB} = 10\log\left(\frac{1}{f_H - f_L}\sum_{f_i=f_L}^{f_H} 10^{\frac{PG_{dB}(f_i)}{10}}\right), \qquad (1)$$

where $PG_{dB}(f_i)$ is the propagation gain in dB measured at a frequency f_i, and f_L and f_H are the lowest and the highest frequencies; and the continuous wave (CW) propagation gains at the center frequency (= 6.85 GHz) were extracted therefrom. Root-mean-square (rms) delay spread was calculated from the time-domain power gain (delay profile) $P(\tau_i)$, where τ_i is the i-th path delay. The rms delay spread (S) is given by

$$S = \sqrt{\frac{\sum_i \tau_i^2 P(\tau_i)}{\sum_i P(\tau_i)} - \left(\frac{\sum_i \tau_i^2 P(\tau_i)}{\sum_i P(\tau_i)}\right)^2}, \qquad (2)$$

where the summations are taken above a threshold level -20 dB below the maximum of $P(\tau_i)$.

A commercially-available device of WiMedia [9] was used in the experiments to facilitate a high data rate and to reduce the fading margin. Its major specifications are listed in Table II. The WiMedia, a high-speed wireless personal area communication standard, utilizes a multiband-OFDM. In OFDM, the input data are divided into blocks of the same size, where each block is referred to as an OFDM symbol. By appending a cyclic prefix to each OFDM symbol, intersymbol interference can be removed as long as the prefix is longer than the impulse response of the channel (typically represented by the delay spread). The multiband-OFDM employs a 60.61-ns zero postfix. When the delay spreads are sufficiently shorter than 60.61 ns, therefore, the WiMedia devices can be used,

TABLE I. SPECIFICATIONS OF THE MICROWAVE VECTOR NETWORK ANALYZER.

Model	Agilent E8362B		
Bandwidth	3.1-10.6 GHz (full-band)	4.2 - 4.8 GHz (low-band)	7.4 -7.9 GHz (high-band)
Frequency sweeping points by VNA	7501	601	501
Calibration	Internal function of the VNA		

TABLE II. PARAMETERS OF A WIMEDIA DEVICE UNDER TEST.

Nominal maximum bit rate	72 Mbps
Modulation	QPSK-OFDM
Frequency	4.2 – 4.8 GHz (low-band) 7.3 – 7.9 GHz (high-band)
Duration of cyclic prefix	60.61 ns

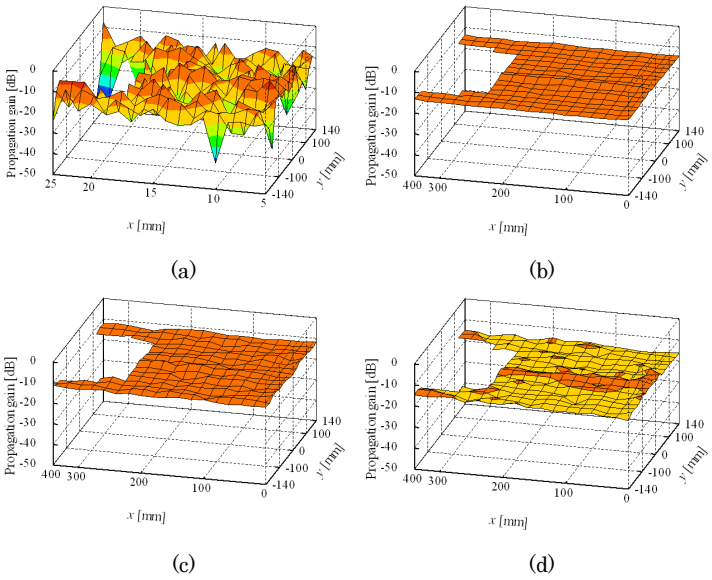

Figure 2. Spatial distribution of propagation gain within the shield box: (a) CW and (b) full-, (c) low-, and (d) high-band UWB.

which yield the maximum data rate of 480 Mbps, within the spacecrafts. Nonetheless, nominal bit rate of the device under test in this paper was 72 Mbps according to specifications.

III. PROPAGATION RESULTS

The spatial distributions of continuous wave (CW) and UWB propagation gains within the shield box are shown in Fig. 2. Since the shield box didn't have a precise symmetry, the propagation gain of CW was asymmetric. Propagation gains ranged -41 — 6.1 dB for CW, -15 — -12 dB for the full-, -14 — -9.7 dB for the low-, and -19 — -13 dB for the high-band UWB. While CW resulted in up to 35 dB fading at several "dead spots" caused by multipath interference, propagation gain variations were 4.7, and 4 dB for full-, low-, and high-band UWB. Spatial distribution of delay spreads for full-band UWB is depicted in Fig. 3. The delay spreads ranged from 43.7

 ISBN: 978-1-61208-453-4

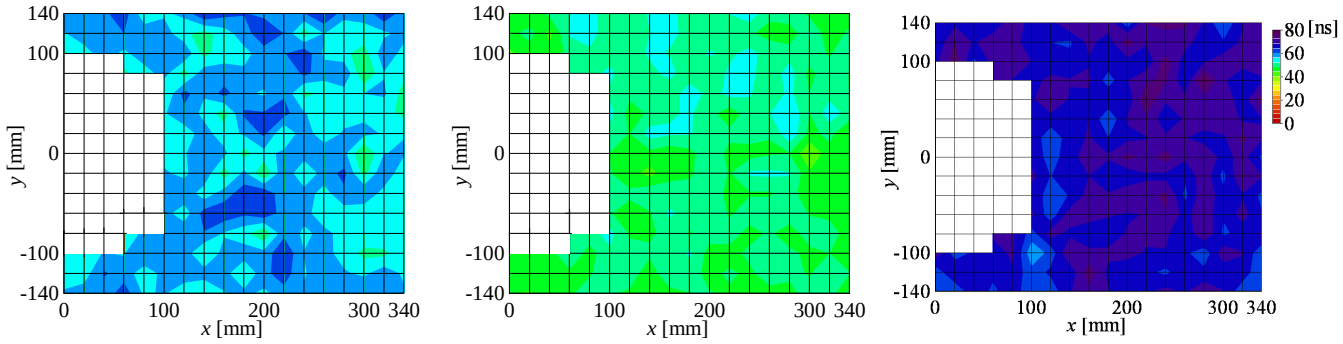

(a) (b) (c)

Figure 3. Spatial distribution of delay spreads for: (a) full- (3.1 - 10.6 GHz), (b) low- (4.2 - 4.8 GHz), and (c) high-band UWB (7.4 - 7.9 GHz).

TABLE III. DIMENSION OF THE INNER VOLUME USED FOR EXPERIMENTS.

	Width [mm]	Depth [mm]	Height [mm]	Volume [m^3]
V	470	430	435	8.8×10^{-2}
V /2			218	4.4×10^{-2}
V /4			108	2.2×10^{-2}
V /8			54	1.1×10^{-2}

to 64.3 ns. The conductive enclosures yields a long delay spread which causes inter-symbol interference, and hence an irreducible error floor when the modulation symbol time is of the same order as the delay spread.

A. *Effects of Volume*

The inner volume (V) of the box was varied between 1.1, 2.2, 4.4, and 8.8×10^{-3} m^3 , as listed in Table III, with use of polystyrene-foam parallelepipeds, covered with aluminium foil and fitted to the bottom of the box. The height of the transmitting and receiving antennas was approximately a half of the box height. Examples of frequency-domain propagation gains are presented measured at (x, y) = (300, 0) with a volume of 1.1×10^{-2} m^3 and 8.8×10^{-2} m^3, in Fig. 4. The frequency- and time-domain gains increase with the inner volume [10]. At a given delay time, a multipath component arrives at the receiving antenna after a different number of reflections on the walls for different-sized boxes, while the traveling time is the same, and hence the total free space propagation loss is the same. The number of reflections increases with decreasing the inner volume, since a mean free path length between reflections is approximately proportional to $V^{1/3}$. Since total reflection losses on the conductive (but not perfectly conductive) walls are roughly proportional to the number of reflections, the propagation gain at a given delay time decreases with increasing inner volume.

The delay spreads were found at more than 85 ns for V = 8.8×10^{-3} m^3, while 5 ns for V = 1.1×10^{-3} m^3. Delay spreads against the inner volume are plotted in Fig. 5 for full-, low-, and high-band UWB. In all cases, the delay spreads increased with the inner volume. Delay profiles at (300, 0) were calculated by the FDTD method and the delay spreads were derived therefrom, when the height was varied between 435, 218, 108, and 54 mm, while the bottom area was fixed at 430 mm × 470 mm. The heights of the antennas were half of the

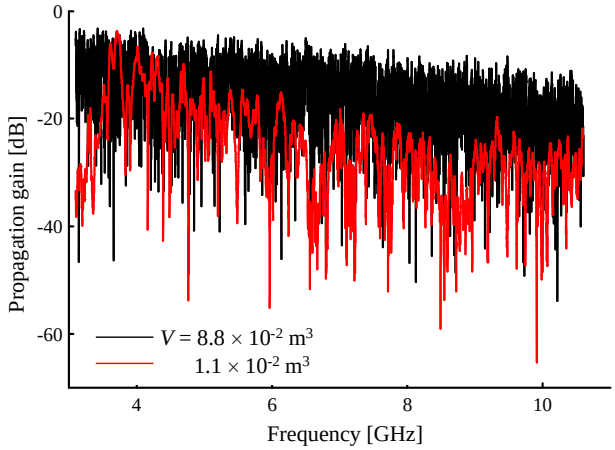

Figure 4. Examples of frequency response measured in the shield boxes (V = 8.8 and 1.1×10^{-2} m^3).

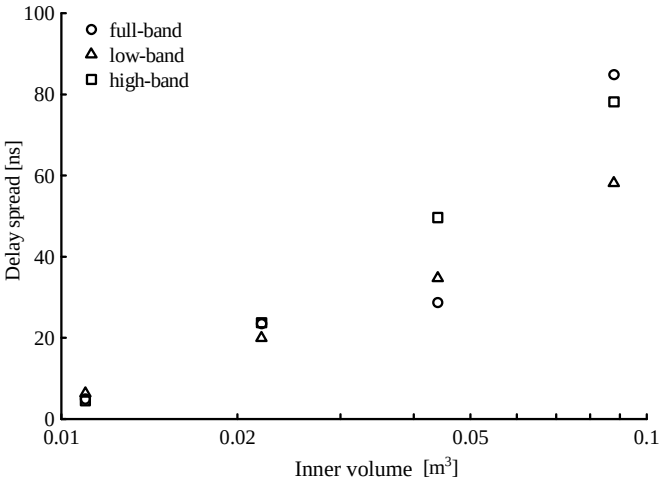

Figure 5. Delay spreads against the inner volume.

inner height of the box. In both cases of simulation and measurement, the delay spreads increased with the inner volume, as shown in Fig. 6. The measurement result is indicated by a circle in Fig. 6. The difference between the simulation and the measurement may be attributed to the electromagnetic energy leakage of the shield box (shielding

 ISBN: 978-1-61208-453-4

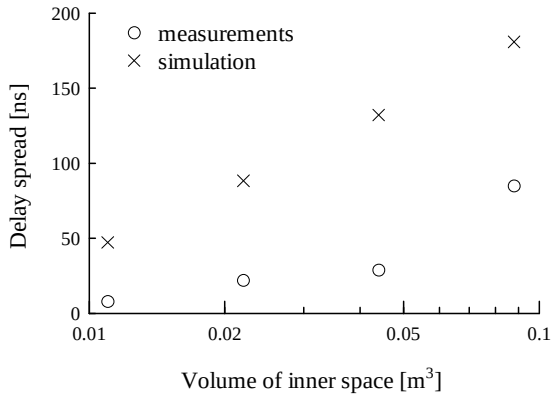

Figure 6. Delay spreads against the inner volume of shield boxes.

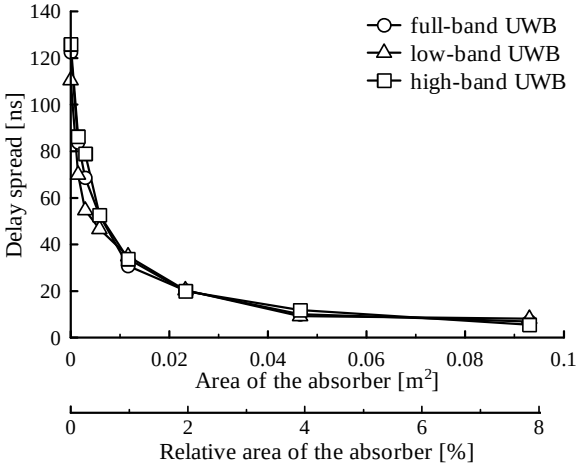

Figure 7. Delay spreads versus area of the absorber.

effectiveness was approximately 60 dB), while the perfect shielding was assumed in the simulation. The longer delay paths were attributed to the heavy multipaths within the conductive closed space.

B. *Effects of Radio Absorber*

A patch of a thin elastic radio absorber was attached at the center of the bottom of the shield box to suppress the delay spreads [5]. The absorbers, 2.3 and 1.8 mm thick, usable in vacuum, attenuated radio wave reflection by 20 dB at 4 and 7 GHz, respectively, and by 10 dB within a 1.5-GHz bandwidth. The absorber of 2.3-mm thickness was used for low-band UWB experiments, and that of 1.8 mm for full- and high-band. Propagation properties were measured while the patch of the strip was 0.093 m^2 (= 305 mm square) × 2^{-n}, where n = 0, 1, 2, …, 6, corresponding 8×2^{-n} % against the total inner surface.

The radio absorber panel can suppress the long delay spreads, as shown in Fig. 7. Received energy losses caused by the radio absorber were estimated: the absorbers of 0.003 m^2 (0.6% against the total inner surface area) and 0.013 m^2 area (4% against the total inner surface area) resulted in 2 and 5 dB

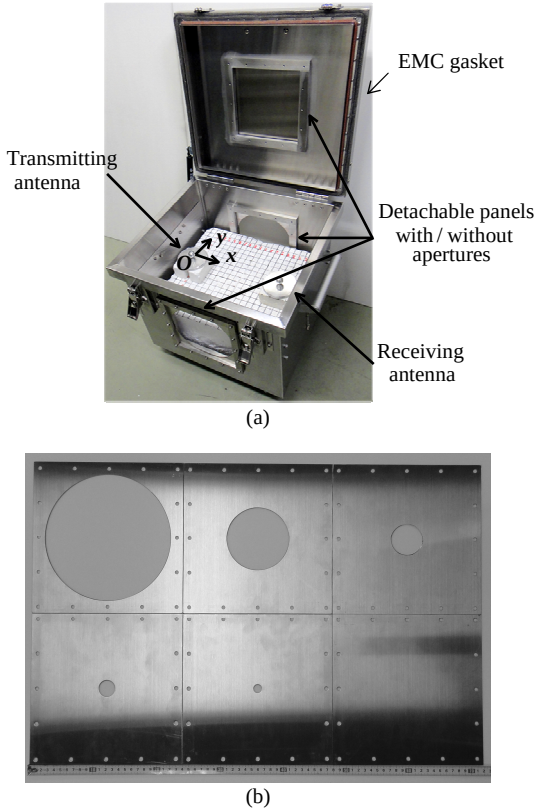

Figure 8. The measurement setup: (a) a shield box had three square holes and (b) panels (240 mm × 240 mm) with and without circular holes.

in energy loss, respectively. Including these energy losses, the relation between the fading depth and the occupied bandwidth was derived, similarly to the case of no absorber. While the absorber panel was places in the center of the bottom of the box in this experiment, Sasaki *et al.* reported that radio reverberation characteristics was almost independent of the position of a small piece of absorber lining within a shielding chamber [11].

C. *Effect of Apertures on the Surface*

The effect of aperture size on UWB propagation was evaluated inside the shield box. The box (the same size of the shield box) had three 200 mm × 200 mm square holes: one in the center of the top lid and the others in the center of both side surfaces, as shown in Fig. 8. For changing total area of apertures, conductive 240 mm × 240 mm square panels with or without circular apertures were attached on the holes with use of conductive gaskets between mating surfaces. The diameter of the circular apertures was 12.5, 25, 50, 100, or 200 mm.

The UWB propagation gains were almost invariable for the total area of apertures normalized by the total area of the inner surface between 0.01 and 0.1%, and gradually decreased with the area beyond 10^{-3} m^2 or 0.1%, as shown in Fig. 9. The lower UWB propagation gains in the high-band UWB were ascribable to longer free space propagation losses. The delay spreads were gradually decreased with the total area of apertures, as shown in Fig. 10. The propagation gain, the delay

profiles, and the delay spreads were found statistically unvaried between the regions near and far from the apertures [12].

IV. TRANSMITTION PERFORMANCE

A commercially-available device of WiMedia [8] was used to measure link throughputs. The link throughputs were measured with use of a pair of WiMedia devices, one of which was links to a solid state drive (SSD) via USB 2.0 interface, and the other was connected to a personal computer with a built-in SSD via a PCMCIA interface. Since the throughputs fluctuated typically ±4 Mb/s per trial, a number of trials (normally 35) were carried out to reduce the variation within ±1 Mb/s.

Throughputs against the inner volume are plotted in Fig. 11 for full-, low-, and high-band UWB. The throughputs decreased with increasing the inner volume, which was attributable to wider delay spreads. The throughput for low- and high-band UWB was up to 96 and 100 Mb/s, when the absorber panel covered 4 and 8% of the total inner surface area, respectively, as shown in Fig. 12. With apertures, the throughputs were almost invariable for the normalized area of apertures between 0.05 and 0.4%, and gradually increased with the area beyond 0.4%, as shown in Fig. 13. When the delay spreads are suppressed sufficiently shorter than the symbol duration, we can use the WiMedia devices, which yield the maximum data rate of 480 Mb/s, within the spacecrafts.

V. CONCLUSIONS

Ultra wideband (from 3.1 — 10.6 GHz, 4.2 — 4.8 GHz, and 7.4 — 7.9 GHz) and CW (6.85 GHz) propagation and transmission were measured and characterized inside a shield box emulating a small spacecraft. While CW resulted in nearly 35-dB fading at several “dead spots” caused by multipath environment, UWB yielded none. The UWB systems have therefore an advantage over narrowband from the viewpoint of reducing fading margins. No dependence on the distance was observed for UWB propagation gain, delay spread, or throughput, and no apparent spatial correlation between them.

The conductive enclosures caused abundant multipaths and long delay spreads. The delay spreads can be suppressed with the use of a small patch of radio absorber and/or with apertures. Propagation gain decreased and the fluctuation range of the gain increased when increasing the area of radio absorber attached on an inner surface. On the other hand, propagation gains were almost invariable for the total area of apertures normalized by the total area of the inner surface between 0.01 and 0.1%, and gradually decreased with the area beyond 0.1%. The higher UWB propagation gains in the high-band UWB were ascribable to higher free space propagation losses. For empty enclosures, an 4% area of radio absorber can suppress the delay spreads less than 10 ns. With 0.1% area of apertures, the delay spreads were found at less than 11 ns. The off-the-shelf WiMedia devices can be used to accommodate up to 480-Mb/s data buses within spacecraft, as long as the delay spread is suppressed far below 60 ns, from the viewpoint of propagation.

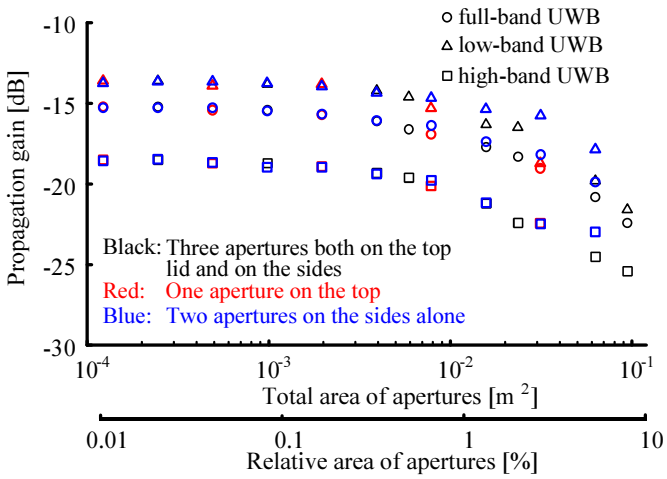

Figure 9. UWB Propagation gains versus total area of apertures.

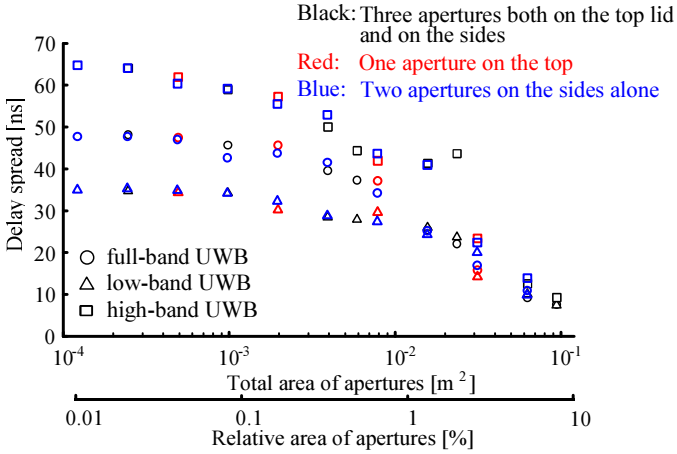

Figure 10. Delay spreads versus total area of apertures.

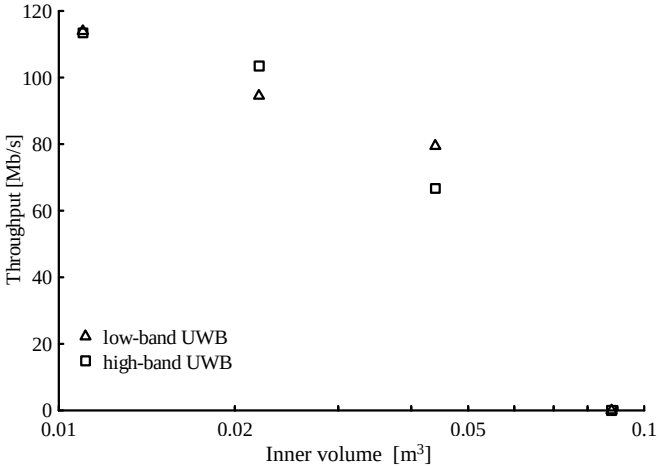

Figure 11. Throughputs against the inner volume.

 ISBN: 978-1-61208-453-4

ACKNOWLEDGMENT

This work was supported by JSPS KAKENHI Grant Number 15J11299.

REFERENCES

[1] T. Kobayashi, “Measurements and characterization of ultra wideband propagation channels in a passenger-car compartment,” *IEICE Trans. Fundamentals*, vol. E89-A, no. 11, pp. 3089-3094, 2006.

[2] M. Ohira, T. Umaba, S. Kitazawa, H. Ban, and M. Ueba, “Experimental characterization of microwave radio propagation in ICT equipment for wireless harness communications,” *IEEE trans. Antennas Propag.*, vol. 59, pp. 4757-4765, Dec. 2011.

[3] J. Gelabert, A. Kavatjikidis, D. J. Edwards, and C. J. Stevens, “Experimental UWB channel characterisation of an electromagnetically small environment,” in *Proc. 2009 Loughborough Antennas and Propagat. Conf. (LAPC 2009)*, pp. 381-384, UK, Nov. 2009.

[4] Z. Li, A. Junshe, X. Yifang, and X. Weiming, “A protocol designed for intra-spacecraft impulse radio ultra-wideband communications,” in *Proc. IEEE Intl. Conf. Wireless for Space and Extreme Environments (WiSEE2014)*, Netherlands, Oct. 2014.

[5] A. Matsubara, A. Tomiki, T. Toda, and T. Kobayashi, “Measurements and characterization of ultra wideband propagation within spacecrafts—proposal of wireless transmission for replacing wired interface buses,” in *Advances in Spacecraft Technologies*, pp. 61-74, IN-TECH, 978-953-307-551-8, Vienna, Austria, Feb. 2011.

[6] P-N. Gineste, Y. Herlem, A. Outay, and P.Pelissou, “Assessment of wireless link budget in a satellite by modelling techniques,” in *2012 ESA Workshop on Aerospace EMC*, pp. 1-6, Venice, Italy, May 2012.

[7] European Cooperation for Space Standardization, Standard ECSS-E-ST-50-12C, “SpaceWire − links, nodes, routers and networks, July 2008.

[8] R. Amini,G. Aalbers,R. Hamann *et al*., “New generations of spacecraft data handling systems:less harness, more reliability,” in *57th Intl. Astronautical Congress (AIAA 2006-448)*, Oct. 2006.

[9] G. Heidari, WiMedia UWB − *Technology of Choice for Wireless USB and Bluetooth*, New York, John Wiley & Sons, 2008.

[10] M. Hirose and T. Kobayashi, “Effects of inner volume on UWB propagation channels within closed spaces,” in *Intl. Conf. on Ultra-Wideband (ICUWB 2014)*, pp. 1-6, France, Aug. 2014.

[11] K. Sasaki, I. Oshima, and Y. Karasawa, “A reverberation chamber to realize multipath-rich environment [II]: Environment control by electromagnetic wave absorbing sheet,” in *IEICE Technical Report A·P2008-9*, pp.13-18, Sep. 2008 (in Japanese).

[12] S. Hamada, A. Tomiki, T. Toda, and T. Kobayashi, “Wireless connections within spacecrafts to replace wired interface buses,” *IEICE Trans. Fandamentals*, vol. E96-A, no. 5, May 2013.

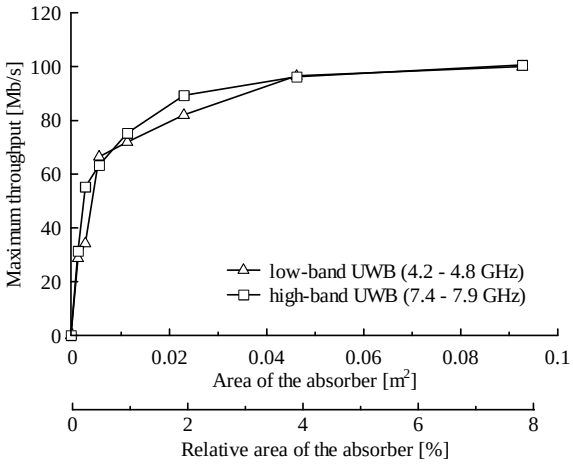

Figure 12. Throughputs measured at (300, 0) versus total area of apertures.

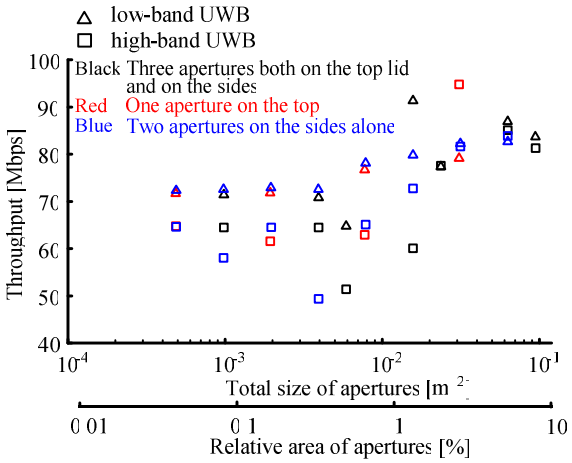

Figure 13. Throughputs measured at (300, 0) versus total area of apertures.

 ISBN: 978-1-61208-453-4